Inorganic Chemistry

Article

pubs.acs.org/IC

Multicopper Models for the Laccase Active Site: Effect of Nuclearity on Electrocatalytic Oxygen Reduction

Edmund C. M. Tse, David Schilter, Danielle L. Gray, Thomas B. Rauchfuss, and Andrew A. Gewirth*

Department of Chemistry, University of Illinois at Urbana−Champaign, 600 South Mathews Avenue, Urbana, Illinois 61801, United States

Supporting Information

ABSTRACT: Cu complexes of 2,2′-dipicolylamine (DPA) were prepared and tested as electrocatalysts for the oxygen reduction reaction (ORR). To study the effect of multinuclearity on the ORR, two Cu−DPA units were connected with a flexible linker, and a third metal-binding pocket was installed in the ligand framework. ORR onset potentials and the diffusion-limited current densities of di- and tricopper complexes of DPA derivatives were found to be comparable to those of the simpler Cu−DPA system. Electrochemical analyses, crystallographic data, and metal-substitution studies suggested that Cu complexes of DPA derivatives reacted with O_2 via a binuclear intermolecular pathway but that the Cu center in the third binding site did not participate in the ORR process. This study highlights the viability of Cu−DPA complexes to mimic the T3-site of laccase, and serves as a guide for designing future laccase models.

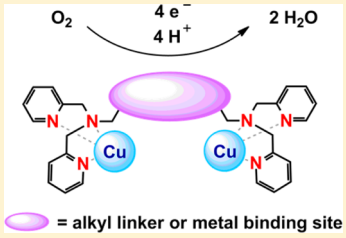

1. INTRODUCTION

Low-temperature polymer electrolyte membrane (PEM) fuel cells represent an attractive power source for clean and sustainable transportation.[1−3] Unlike conventional combustion engines, fuel cells do not exhibit the Carnot limitation on the conversion of heat to mechanical work.[4,5] The development of fuel cells has been hampered by several design issues.[6−10] From a technical standpoint, the key to fuel cell viability is efficient mediation of the oxygen reduction reaction (ORR) to water: $O_2 + 4\ e^- + 4\ H^+ \rightarrow 2\ H_2O$.[11] Presently, cathodes of choice feature Pt or one of its alloys, these being neither cheap nor sufficiently active and robust.[12−15]

Synthetic Cu complexes exhibit rich reactivity toward O_2, and several Cu−O_2 binding modes have been identified for mono- and multicopper systems.[16−21] In view of the essential role of Cu in O_2-activating enzymes,[22] it is no surprise that Cu complexes have been well-studied in the context of ORR catalysis.[23] For example, the facile oxygenation of $[Cu(TPA)]^+$ (tris(2-pyridylmethyl)amine = TPA) and its derivatives led to the discovery that $[Cu(TPA)(H_2O)]^{2+}$ complex has the lowest ORR overpotential at pH 1 of any synthetic Cu catalysts.[24−26] Through pyrolysis and reconstitution studies, we showed that ORR activity necessitates the Cu centers to be attached to the *N*-donor ligands.[27] Further studies, however, showed that variations of the TPA platform do not strongly affect the ORR onset potential, even though the Cu(I/II) couple is affected.[27] In view of the modest effects of substituents on ORR catalysis by the Cu−TPA platform, further development requires more drastic changes in the design of catalysts based on the Cu−TPA motif.

The design of new ORR catalysts could benefit from more faithful mimicry of biological catalysts for the same reaction. Cu enzymes catalyze the four-electron reduction of O_2 to water very efficiently.[28−30] Often found in fungi (e.g., *Melanocarpus albomyces*,[31] *Rigidoporus lignosus*,[32] and *Trametes versicolor*[33]), laccases are ORR catalysts that feature a characteristic tricopper O_2-binding site supplemented by a fourth Cu center. Upon immobilization onto an electrode, laccase exhibits an ORR overpotential of only ∼100 mV, which is even better than Pt-based catalysts.[23,34−39] However, due to the large size of laccase (160 nm^3),[33,40,41] electrodes decorated with these enzymes cannot deliver the power densities required for practical use.[42] Furthermore, laccases denature under operating conditions typical of PEM fuel cells.[43,44] Synthetic models of the trinuclear Cu active site could possibly replicate the high activity of laccase while exhibiting the durability and power density necessary for PEM fuel cell applications.[5] Such functional tricopper active site models have, however, not yet been reported.[45]

The laccase active site features two Cu centers each bound to three histidine residues (denoted "T3" sites) and a third Cu existing in a pocket with two histidine ligands, a "T2" site (Figure 1a).[46] The tricopper O_2-binding site is dynamic, i.e. the Cu−Cu distances change from ∼5 Å in the fully reduced state to ∼3.5 Å in the oxygenated state.[31,33,45] Synthetic tricopper complexes often form very stable μ_3-hydroxy species, e.g. $[Cu^{II}_3(\mu_3\text{-}OH)(trz)_3(OH)_2(H_2O)_4]\cdot 4.5\ H_2O$ (Htrz =1,2,4-triazole) and $[Cu_3(\mu_3\text{-}OH)(\mu\text{-}pz)_3(HCOO)_2(Hpz)_2]$ (Hpz = pyrazole), such motifs typically being inactive toward ORR.[47,48] The design of appropriately ligated tricopper catalysts thus remains an unsolved area of research. Whereas many ligand scaffolds feature three equivalent Cu binding sites, few designs replicate the asymmetry of the laccase active site.[49]

In addition to the tricopper site that binds O_2, laccase features a fourth copper, labeled T1. When the T1 site (not

Received: May 8, 2014
Published: July 29, 2014

   dx.doi.org/10.1021/ic501080c | Inorg. Chem. 2014, 53, 8505−8516

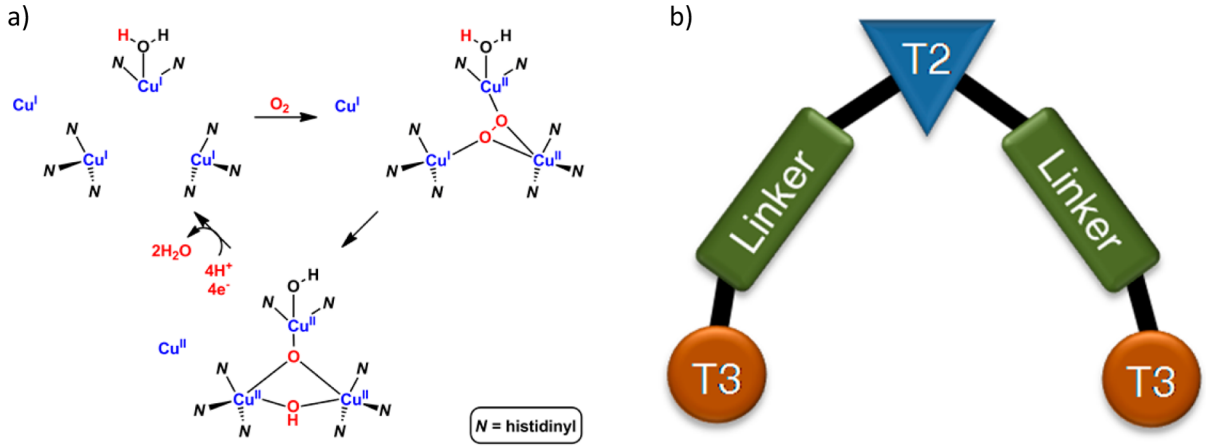

Figure 1. (a) Schematic of the laccase active site,[46] and (b) design principle for models of the laccase tricopper site.

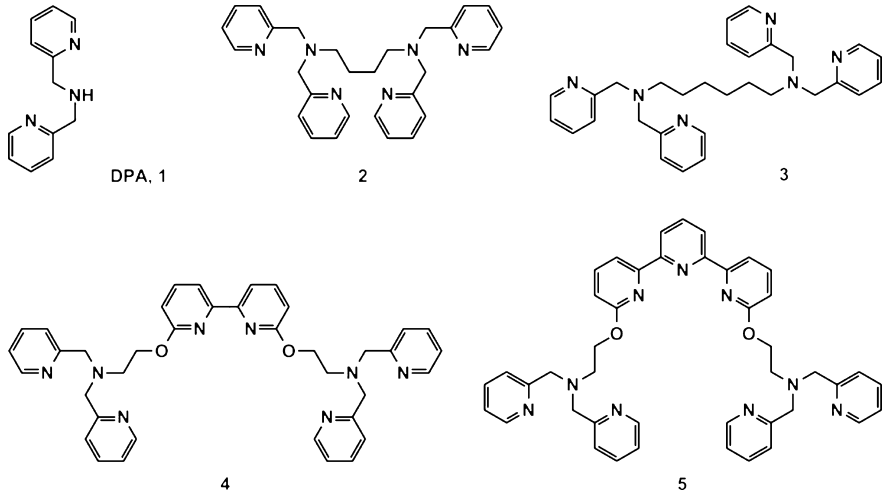

Figure 2. Ligands used in this study: 2,2′-dipicolylamine (DPA, **1**), *N,N,N′,N′*-tetra(pyridin-2-ylmethyl)butane-1,4-diamine (**2**), *N,N,N′,N′*-tetra(pyridin-2-ylmethyl)hexane-1,6-diamine (**3**), 2,2′-([2,2′-bipyridine]-6,6′-diylbis(oxy))bis(*N,N*-bis(pyridin-2-ylmethyl)ethanamine) (**4**), and 2,2′-([2,2′:6′,2″-terpyridine]-6,6″-diylbis(oxy))bis(*N,N*-bis(pyridin-2-ylmethyl)ethanamine) (**5**).

depicted) is substituted with Hg(II), which is redox-inactive, laccase loses its catalytic activity, although it still binds but does not cleave O_2.[50] The T1 copper functions as an electron reservoir, which can in principle be replicated with an electrode in model systems.

In this report we describe initial efforts to construct and test ensembles of T2 and T3 sites, as inspired by laccase. Figure 1b shows our design concept for the laccase active site: T2 and T3 sites are connected by flexible linkers. The T3 centers feature coordination of Cu by three *N*-donor groups, while the T2 center features Cu coordination by two *N*-donor groups. Given the high ORR activity afforded by the TPA ligand,[26,27] its derivative, 2,2′-dipicolylamine (DPA, **1**) was used to simulate the T3 site mimics while we used 2,2′-bipyridine (bipy) and 2,2′:6′,2″-terpyridine (terpy) for the T2 site mimic. Figure 2 shows the ligands used in this study (including the new species **4**, a prototypical T3−T2−T3 mimic), each of which incorporates DPA fragments as surrogates for the native tris(imidazolyl) binding pockets.

2. EXPERIMENTAL SECTION

Materials and Methods. Unless otherwise stated, all chemicals were purchased from commercial sources and used as received. The ligands *N,N,N′,N′*-tetra(pyridin-2-ylmethyl)butane-1,4-diamine (**2**) and *N,N,N′,N′*-tetra(pyridin-2-ylmethyl)hexane-1,6-diamine (**3**) were prepared according to a published procedure,[51] using NMe_4I instead of $[N(C_{12}H_{25})Me_3]Cl$ as the catalyst. The trinucleating ligand 2,2′-([2,2′:6′,2″-terpyridine]-6,6″-diylbis(oxy))bis(*N,N*-bis(pyridin-2-ylmethyl)ethanamine) (**5**) and its tricopper complex $[Cu_3Cl_6(\mathbf{5})]$ were also prepared using a modified literature procedure, using KO^{t}Bu in THF instead of KOH in DMSO.[52] The monocopper complexes $[Cu(\mathbf{1})](NO_3)_2$ and $[Cu(\mathbf{1})Cl_2]$ were prepared following literature methods.[53,54] Degassed MeCN and THF were dried through columns of activated alumina and stored over molecular sieves. ^{1}H NMR spectra were recorded on a Varian VXR500 spectrometer at 500 MHz. A Waters Micromass Quattro II spectrometer was used to acquire ESI-MS data for analytes in dilute MeOH solution. CHN analytical data were acquired using an Exeter Analytical CE-440 elemental analyzer.

Synthesis and Characterization. *2,2′-([2,2′-Bipyridine]-6,6′-diylbis(oxy))bis(N,N-bis(pyridin-2-ylmethyl)ethanamine) (**4**).* Under an atmosphere of dry N_2, a stirred solution of *N,N′*-di(2-picolyl)-ethanolamine (73.0 mg, 0.300 mmol) in THF (1 mL) was treated with KO^{t}Bu (37.0 mg, 0.330 mmol) suspended in THF (2 mL). After 30 min, 6,6′-dibromo-2,2′-bipyridine (31.4 mg, 0.100 mmol) suspended in THF (2 mL) was added and the mixture stirred for 96 h at room temperature, before the mixture was heated and the solvent boiled off. The oily residue was extracted with CH_2Cl_2 (5 mL), and the solution was washed with H_2O (3 × 10 mL), dried over Na_2SO_4, and evaporated to dryness to leave a pale oil. Recrystallization from warm Me_2CO afforded the product as off-white plates (42.2 mg, 66.0 μmol, 66%). ^{1}H NMR ($CDCl_3$): 8.49 (m, 4H, py-H6), 7.80 (m, 2H, bipy-

dx.doi.org/10.1021/ic501080c | Inorg. Chem. 2014, 53, 8505−8516

H3), 7.65−7.50 (m, 10H, py-H3,4/bipy-H4), 7.10 (m, 4H, py-H5), 6.69 (m, 2H, bipy-H5), 4.58 (t, $^3J_{HH}$ = 6 Hz, 4H, OCH_2), 3.99 (s, 8H, pyCH_2), 3.08 (t, $^3J_{HH}$ = 6 Hz, 4H, OCH$_2$CH_2) ppm. ESI-MS: *m/z* 639.3 [M + H]$^+$, 320.4 [M + 2H]$^{2+}$. Anal. Calcd for $C_{38}H_{38}N_8O_2$: C, 71.45; H, 6.00; N, 17.54. Found: C, 71.32; H, 5.97; N, 16.82.

*[Cu(MeCN)(**1**)]BF$_4$.* Under an atmosphere of dry N_2, [Cu(MeCN)$_4$]BF$_4$ (62.9 mg, 200 μmol) and **1** (39.9 mg, 200 μmol) were dissolved in MeCN (2 mL) with stirring. After 10 min, the solution was layered with Et_2O (15 mL) and allowed to stand at −28 °C for 1 h. The solid was isolated by filtration, washed with Et_2O (2 × 2 mL), and dried briefly to give the title compound as a yellow microcrystalline powder (68.8 mg, 176 μmol, 88%). ^{1}H NMR (CD_3CN) 8.56 (m, 2H, H6), 7.80 (m, 2H, H4), 7.36 (m, 2H, H5), 7.32 (m, 2H, H3), 4.03 (s, 4H, CH_2), 3.87 (s, 1H, N*H*), 1.96 (s, CH_3) ppm. ESI-MS: *m/z* 303.0 [M − BF_4^-]$^+$, 262.0 [M − MeCN − BF_4^-]$^+$. Anal. Calcd for $C_{14}H_{16}BCuF_4N_3$−MeCN: C, 41.23; H, 3.75; N, 12.02. Found: C, 41.22; H, 3.68; N, 11.79 (the MeCN ligand is readily lost under vacuum).

*[Cu$_2$(MeCN)$_2$(**2**)](BF$_4$)$_2$.* Under an atmosphere of dry N_2, [Cu(MeCN)$_4$]BF$_4$ (251.6 mg, 800 μmol) and **2** (192.3 mg, 400 μmol) were dissolved in MeCN (5 mL) with stirring. After 2 h, the solution was layered with Et_2O (15 mL) and allowed to stand at −28 °C for 1 h. The solid that formed was isolated by filtration, washed with Et_2O (2 × 2 mL), and dried briefly to give the title compound as a yellow microcrystalline powder (325.1 mg, 389 μmol, 97%). ^{1}H NMR (CD_3CN): d8.56 (d, $^3J_{HH}$ = 5.0 Hz, 4H, H6), 7.83 (dt, $^3J_{HH}$ = 7.7 Hz, $^4J_{HH}$ = 1.7 Hz, 4H, H4), 7.41 (t, $^3J_{HH}$ = 6.3 Hz, 4H, H5), 7.35 (d, $^3J_{HH}$ = 7.8 Hz, 4H, H3), 3.79 (s, 8H, pyCH_2), 2.70 (t, $^3J_{HH}$ = 7.4 Hz, 4H, NCH_2), 1.97 (s, 6H, CH_3), 1.56 (m, 8H, NCH$_2$CH_2) ppm. ESI-MS: *m/z* 665.1 [M − MeCN − BF_4^-]$^+$, 309.6 [M − 2BF_4^-]$^{2+}$, 289.1 [M − MeCN − 2BF_4^-]$^{2+}$. Anal. Calcd for $C_{32}H_{38}B_2Cu_2F_8N_8$·0.5MeCN: C, 46.31; H, 4.65; N, 13.91. Found: C, 46.44; H, 4.72; N, 13.84.

*[Cu$_2$(MeCN)$_2$(**3**)](BF$_4$)$_2$.* This compound was prepared analogously to [Cu$_2$(MeCN)$_2$(**2**)](BF$_4$)$_2$, instead using **3** as the precursor. A sticky golden semisolid was obtained, which was purified by crystallization from MeCN/Et_2O. Yield: 92%, yellow powder. ^{1}H NMR (CD_3CN): 8.57 (m, 4H, H6), 7.84 (t, $^3J_{HH}$ = 6.9 Hz, 4H, H4), 7.41 (t, $^3J_{HH}$ = 6.1 Hz, 4H, H5), 7.36 (d, $^3J_{HH}$ = 7.3 Hz, 4H, H3), 3.80 (s, 8H, pyCH_2), 2.70 (t, $^3J_{HH}$ = 7.8 Hz, 4H, NCH_2), 1.96 (s, 6H, CH_3), 1.54 (m, 8H, NCH$_2$CH_2), 1.20 (m, 8H, NCH$_2$CH$_2$CH_2) ppm. ESI-MS: *m/z* 693.0 [M − MeCN − BF_4^-]$^+$, 303.0 [M − MeCN − 2BF_4^-]$^{2+}$. Anal. Calcd for $C_{34}H_{42}B_2Cu_2F_8N_8$: C, 47.29; H, 4.90; N, 12.98. Found: C, 46.96; H, 4.82; N, 12.66.

*[Cu$_2$(NO$_3$)$_4$(**2**)].* A solution of Cu(NO$_3$)$_2$·2.5H$_2$O (93.0 mg, 400 μmol) in boiling MeOH (1 mL) was treated with **2** (90.5 mg, 200 μmol) in MeOH (2 mL) with stirring. A pale-blue solid precipitated from the deep-blue mixture. Upon cooling to room temperature, the solid was isolated by filtration and washed with MeOH (2 mL) to give the product as a blue microcrystalline powder (157.3 mg, 190 μmol, 95%). ESI-MS: *m/z* 764.6 [M − NO_3^-]$^+$. Anal. Calcd for $C_{28}H_{32}Cu_2N_{10}O_{12}$: C, 40.63; H, 3.90; N, 16.92. Found: C, 40.57; H, 3.81; N, 16.43.

*[Cu$_2$(NO$_3$)$_4$(**3**)].* This compound was prepared analogously to [Cu$_2$(NO$_3$)$_4$(**2**)], instead using **3** as the precursor. Yield: 96%, blue powder. ESI-MS: *m/z* 792.6 [M − NO_3^-]$^+$, 365.3 [M − 2NO_3^-]$^{2+}$. Anal. Calcd for $C_{30}H_{36}Cu_2N_{10}O_{12}$·1.25H$_2$O: C, 41.03; H, 4.42; N, 15.95. Found: C, 41.09; H, 4.27; N, 15.48.

*[Cu$_2$Cl$_4$(**2**)].* A solution of CuCl$_2$·2H$_2$O (68.2 mg, 400 μmol) in boiling MeOH (1 mL) was treated with **2** (90.5 mg, 200 μmol) in MeOH (2 mL) with stirring. Upon cooling to room temperature, the deep-blue mixture was treated with Et_2O (15 mL) and the resulting solid isolated by filtration and washed with Et_2O (2 mL) to give the product as a baby blue crystals (127.1 mg, 176 μmol, 88%). ESI-MS: *m/z* 685.5 [M − Cl^-]$^+$, 325.4 [M − 2Cl^-]$^{2+}$. Anal. Calcd for $C_{28}H_{32}Cl_4Cu_2N_6$·2MeOH: C, 44.84; H, 5.27; N, 10.46. Found: C, 45.15; H, 5.15; N, 10.36.

*[Cu$_2$Cl$_4$(**3**)].* This compound was prepared analogously to [Cu$_2$Cl$_4$(**2**)], instead using **3** as the precursor. Yield: 85%, teal powder. ESI-MS: *m/z* 712.7 [M − Cl^-]$^+$. Anal. Calcd for $C_{30}H_{36}Cl_4Cu_2N_6$·0.5H$_2$O: C, 47.50; H, 4.92; N, 11.08. Found: C, 47.53; H, 4.90; N, 10.75. Blue prisms of [Cu$_2$Cl$_4$(**3**)]·2MeOH formed upon slow diffusion of Et_2O vapor into a MeOH solution of the title compound. One crystal (0.493 × 0.308 × 0.202 mm^3) was subjected to X-ray diffraction studies.

*[Cu$_2$(ClO$_4$)$_4$(**2**)].* Cu(ClO$_4$)$_2$·6H$_2$O (74.1 mg, 200 μmol) in boiling MeOH (1 mL) was treated with **2** (45.3 mg, 100 μmol) in MeOH (1 mL) with stirring. Upon cooling to room temperature, the deep-blue mixture was treated with Et_2O (15 mL) and the resulting solid isolated by filtration and washed with Et_2O (2 mL) to give the product as a purple microcrystalline powder (93.4 mg, 95.6 μmol, 96%). ESI-MS: *m/z* 877.4 [M − ClO_4^-]$^+$, 389.4 [M − 2ClO_4^-]$^{2+}$. Anal. Calcd for $C_{28}H_{32}Cl_4Cu_2N_6O_{16}$·7H$_2$O: C, 30.47; H, 4.20; N, 7.62. Found: C, 30.46; H, 3.65; N, 7.16.

*[Cu$_2$(ClO$_4$)$_4$(**3**)].* This compound was prepared analogously to [Cu$_2$(ClO$_4$)$_4$(**2**)], instead using **3** as the precursor. Addition of Et_2O was not required to precipitate the product. Yield: 82%, blue powder. ESI-MS: *m/z* 905.0 [M − ClO_4^-]$^+$, 403.0[M − 2ClO_4^-]$^{2+}$. Anal. Calcd for $C_{30}H_{36}Cl_4Cu_2N_6O_{16}$·4H$_2$O: C, 33.44; H, 4.12; N, 7.80. Found: C, 33.40; H, 3.93; N, 7.68.

*[Cu$_4$(OH)$_4$(**2**)$_2$](BF$_4$)$_4$.* Under an atmosphere of dry N_2, [Cu$_2$(MeCN)$_2$(**2**)](BF$_4$)$_2$ (83.5 mg, 100 μmol) was dissolved in MeCN (1 mL). The solution was then cooled to −78 °C and placed under O_2 (1 atm), after which the solution, now a blue-green color, was allowed to warm to room temperature. The solution was treated with Et_2O (5 mL) and allowed to stand at −28 °C for 1 h, the resulting solid was isolated by filtration, washed with Et_2O (2 × 2 mL), and dried briefly to give the title compound as blue-green crystals (71.7 mg, 45.6 μmol, 91%). ESI-MS: *m/z* 699.2 [M − 2BF_4^-]$^{2+}$, 437.9 [M − 3BF_4^-]$^{3+}$, 306.6 [M − **2** − 2Cu^{2+} − 2OH^- − 4BF_4^-]$^{2+}$. Anal. Calcd for $C_{56}H_{68}B_4Cu_4F_{16}N_{12}O_4$·H$_2$O: C, 42.23; H, 4.43; N, 10.55. Found: C, 41.92; H, 4.17; N, 10.25.

*[Cu$_4$(OH)$_4$(**3**)$_2$](BF$_4$)$_4$.* This compound was prepared analogously to [Cu$_4$(OH)$_4$(**2**)$_2$](BF$_4$)$_4$, instead using [Cu$_2$(MeCN)$_2$(**3**)](BF$_4$)$_2$ as the precursor. Yield: 87%, blue-green crystals. ESI-MS: *m/z* 727.0 [M − **3** − 2Cu^{2+} − 2OH^- − 3BF_4^-]$^+$, 320.0 [M − **3** − 2Cu^{2+} − 2OH^- − 4BF_4^-]$^{2+}$. Anal. Calcd for $C_{60}H_{76}B_4Cu_4F_{16}N_{12}O_4$: C, 43.24; H, 4.84; N, 10.08. Found: C, 43.43; H, 4.42; N, 9.69. Blue prisms of [Cu$_4$(OH)$_4$(**3**)$_2$](BF$_4$)$_4$·4MeCN·4H$_2$O formed upon slow diffusion of Et_2O vapor into a MeCN solution of the title compound. One crystal (0.1323 × 0.0621 × 0.0435 mm^3) was subjected to X-ray diffraction studies.

*[Cu$_2$Cl$_4$(**4**)].* CuCl$_2$·2H$_2$O (17.0 mg, 100 μmol) in MeOH (0.5 mL) was treated with **4** (31.9 mg, 50 μmol) in warm MeOH (1 mL) with stirring. The blue solution was treated with Et_2O (15 mL), and the resulting solid that formed was isolated by filtration, washed with Et_2O (2 mL), and dried briefly to give the product as a baby-blue powder (42.7 mg, 47 μmol, 94%). ESI-MS: *m/z* 871.2 [M − Cl^-]$^+$, 418.0 [M − 2Cl^-]$^{2+}$.

*[Cu$_3$Cl$_6$(**4**)].* This compound was prepared analogously to [Cu$_3$Cl$_6$(**5**)], instead using **4** as the precursor. Yield: 81%, blue-green powder. ESI-MS: *m/z* 1005.8 [M − Cl^-]$^+$, 971.0 [M − Cl − Cl^-]$^+$, 871.0 [M − Cu^{2+} − Cl^-]$^+$, 485.5 [M − 2Cl^-]$^{2+}$, 418.0 [M − Cu^{2+} − 4Cl^-]$^{2+}$.

*[Cu$_2$Ag(NO$_3$)$_5$(**4**)].* Cu(NO$_3$)$_2$·2.5H$_2$O (23.3 mg, 100 μmol) and $AgNO_3$ (8.5 mg, 50 μmol) in MeOH (1 mL) were treated with **4** (31.9 mg, 50 μmol) in warm MeOH (1 mL) with stirring in the absence of light. After 5 min, the teal mixture was treated with Et_2O (15 mL) and allowed to stand overnight in the absence of light. The solid that formed was isolated by filtration, washed with Et_2O (2 mL), and dried briefly to give the product as a green microcrystalline powder (49.9 mg, 42 μmol, 84%). ESI-MS: *m/z* 1121.2 [M − NO_3^-]$^+$, 529.5 [M − 2NO_3^-]$^{2+}$. Anal. Calcd for $C_{28}H_{32}Cl_4Cu_2N_6O_{16}$·MeOH: C, 38.53; H, 3.48; N, 14.98. Found: C, 38.59; H, 3.06; N, 14.48.

Caution! Perchlorate salts of metal ion complexes are potentially explosive. Only small amounts of materials should be prepared.

General Method for Ink Preparation. A suspension of finely ground Vulcan XC-72 (90 mg, Cabot Corp.) and Cu(ClO$_4$)$_2$·6H$_2$O (18.5 mg, 50.0 μmol) in boiling MeOH (2 mL) was treated with ligand **1** (50.0 μmol), **2**/**3** (25.0 μmol), or **4**/**5** (16.7 μmol) in MeOH (1 mL). The mixture was briefly sonicated and treated with Et_2O (15

dx.doi.org/10.1021/ic501080c | *Inorg. Chem.* 2014, 53, 8505−8516

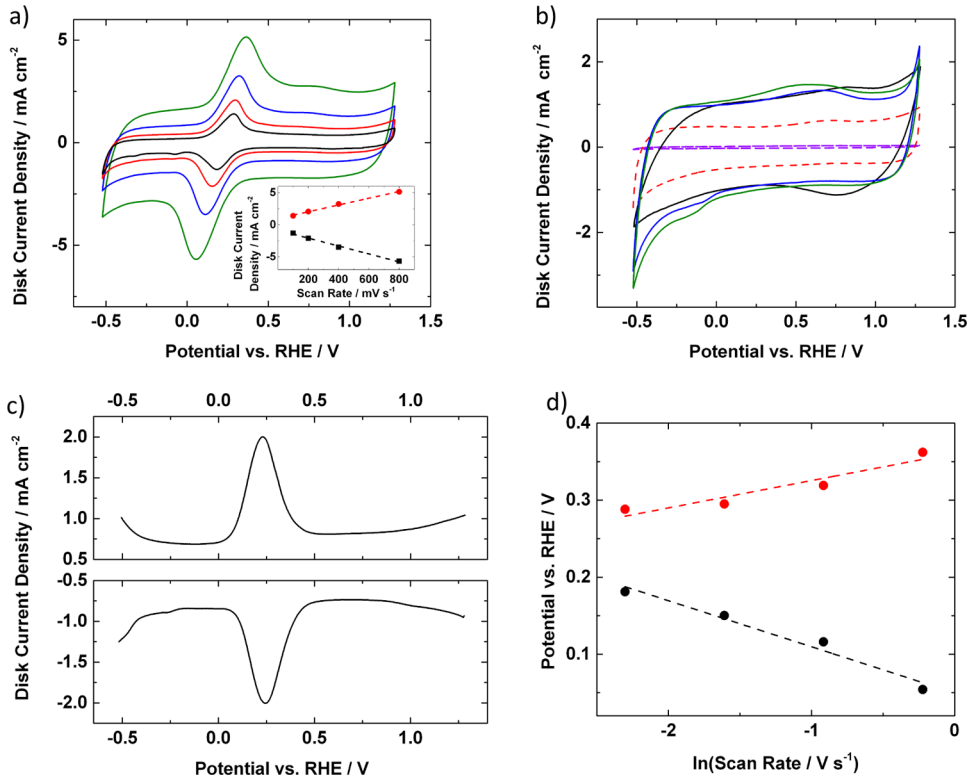

Figure 3. (a) Cyclic voltammograms (CVs) of $[Cu(\mathbf{1})]^{2+}$ with scan rates of 100 (black), 200 (red), 400 (blue), 800 (green) mV/s. Randles−Sevcik plots (inset) of $[Cu(\mathbf{1})]^{2+}$ projected from the cathodic (black dots) and anodic (red dots) peak current densities. (b) CVs of **1** (black), **3** (blue), **4** (green), Vulcan-XC72 blank (red, dash), and bare GC electrode (purple, dash) with scan rates of 200 mV/s. (c) Differential pulse voltammogram (DPV) of $[Cu(\mathbf{1})]^{2+}$. (d) Plot of cathodic (black) and anodic (red) peak potential of $[Cu(\mathbf{1})]^{2+}$ vs natural log of scan rate. Studies were conducted in pH 4 Ar-sparged Britton-Robinson buffer.

mL), and the solids were isolated by centrifugation before being dried in vacuo (80 °C, 3 h). A fraction (3.6 mg) of the resulting carbon-supported catalyst was suspended in EtOH (1 mL) and treated with Nafion (4 μL, 5 wt % in alcohols, Sigma-Aldrich), the resulting slurry being sonicated for 30 min. This ink (10 μL) was then deposited on a glassy carbon (GC) electrode, which was dried under a stream of Ar.

Ink Preparation for Anion Effect Study. Inks of monocopper complexes were prepared from *in situ* generated species. Thus, solutions of **1** (3.4 mg, 17 μmol) in EtOH (2.5 mL) were treated separately with $Cu(ClO_4)_2{\cdot}6H_2O$ (6.3 mg, 17 μmol), $Cu(NO_3)_2{\cdot}2.5H_2O$ (4.0 mg, 17 μmol), $CuSO_4{\cdot}5H_2O$ (4.2 mg, 17 μmol), $CuCl_2$ (2.3 mg, 17 μmol), $Cu(HCO_2)_2{\cdot}xH_2O$ (4.0 mg, ~17 μmol) and $Cu(OAc)_2{\cdot}H_2O$ (3.4 mg, 17 μmol). After sonicating each solution for 10 min, finely ground Vulcan XC-72 (9 mg, Cabot Corp.) was added, and the suspensions were sonicated for a further 10 min. A solution of Nafion (10 μL, 5 wt % in alcohols, Sigma-Aldrich) was added to the suspensions, and the resulting slurries were sonicated for 30 min. The inks (10 μL) were then deposited on a GC electrode, which was dried under a stream of Ar.

Electrochemical Experiments. Aqueous solutions were prepared using Milli-Q purified water (>18 MΩ cm^{-1}). Experiments at pH 1 and 13 were performed in $HClO_4$ (0.1 M, 70 wt % optima grade $HClO_4$, Fisher Scientific) and in NaOH (0.1 M, analytical titration grade, Fisher Scientific) diluted with Milli-Q water, respectively. Experiments at pH 4−10 were performed in Britton-Robinson buffer consisting of H_3BO_3 (0.04 M, 99.999%, Sigma-Aldrich), CH_3COOH (0.04 M, 99.99%, Sigma-Aldrich), H_3PO_4 (0.04 M, 85 wt % in H_2O, 99.99%, Sigma-Aldrich), and $NaClO_4$ (0.1 M, 99.9%, Sigma-Aldrich). The pH was adjusted to 4, 7, and 10 using NaOH (10 M, analytical titration grade, Fisher Scientific). Solutions were sparged with Ar or O_2 for 30 min prior to each experiment.

Electrochemical studies were carried out using a CH Instruments 760 D Electrochemical Workstation (Austin, TX) at room temperature. Experiments were performed in a three-compartment cell with an aqueous "no leak" Ag/AgCl (3 M KCl, ESA, Inc.) reference electrode separated from the working electrode by a Luggin capillary. Electrochemical potentials are reported relative to the reversible hydrogen electrode by sparging the solution with H_2 (1 atm) and monitoring the open circuit potential. A carbon rod counter electrode was separated from the working electrode by a glass frit.

Rotating ring-disk electrode (RRDE) experiments were performed using a ring-disk assembly with an interchangeable disk (E5 series, Pine instruments) connected to a MSRX rotator (Pine Instruments). The GC disk electrode (A = 0.196 cm^2) was polished sequentially with 0.25 and 0.05 μm diameter diamond polish (Buehler), and sonicated in water after each stage. The Pt ring electrode (A = 0.093 cm^2, Pine Instruments) was cleaned electrochemically by cycling from −0.4 V to +1.7 V vs Ag/AgCl reference at 100 mV/s in an aqueous solution of $HClO_4$ (0.1 M) until the current of oxide stripping at ~+0.35 V vs Ag/AgCl reference remained constant. A GC electrode was used as a standard for the 2 e^- reduction of O_2. The collection efficiency of the ring electrode, which was held at 1.2 V vs RHE, was determined to be 15.5%.

Structure Determination. Single-crystal X-ray diffraction data were collected on compounds $[Cu_2Cl_4(\mathbf{3})]{\cdot}2H_2O$ and $[Cu_4(OH)_4(\mathbf{3})_2](BF_4)_4{\cdot}4MeCN{\cdot}4H_2O$ with the use of graphite-monochromatized Mo Kα radiation (λ = 0.71073 Å) at 168 and 183 K, respectively. For each crystal, four ω scan frame series were collected on a Bruker platform APEX II CCD diffractometer.[55] Intensity data collection, cell refinement, and data reduction were carried out with the APEX2 suite of programs.[55] Face-indexed absorption corrections were performed numerically with the use of the program XPREP.[56] Then the program SADABS was employed to make incident beam and decay corrections.[56] The structures were solved with the direct methods program SHELXS and refined with the full-matrix least-squares program SHELXL of the SHELXTL suite of

dx.doi.org/10.1021/ic501080c | Inorg. Chem. 2014, 53, 8505−8516

programs.[57] Both structures contained disordered solvate molecules whose positions could not be solved, so the "squeeze" routine in the program Platon was used to remove the solvate contributions from the structures.[58] Additional experimental details and selected metrical data are shown in Tables S1−2 in the Supporting Information (SI).

3. RESULTS AND DISCUSSION

3.1. Cu Complex of DPA as T3 Site Mimic.

3.1.1. Voltammetry under Ar. Toward a functional model of laccase, we tested the feasibility of using $[Cu(\mathbf{1})]^{2+}$ to mimic the T3 unit of the tricopper active site. We collected voltammograms of $[Cu(\mathbf{1})]^{2+}$ (Figure 3a) and **1** (Figure 3b, black trace), both supported on XC-72 carbon in Ar-sparged pH 4 Britton-Robinson buffer. Whereas free DPA and other DPA derivatives are redox-inactive, $[Cu(\mathbf{1})]^{2+}$ exhibits a reversible wave at a midpoint potential $E_{1/2}$ = +0.23 V vs RHE, this wave being assigned to the Cu(I/II) couple. This behavior is comparable to that for $[Cu(TPA)(H_2O)]^{2+}$ ($E_{1/2}$ = +0.23 V) studied previously.[26] Differential pulse voltammetry (DPV) shows a single redox wave centered at +0.23 V (Figure 3c), confirming the peak observed by cyclic voltammetry (CV).

The inset to Figure 3a shows the Randles−Sevcik plot obtained for $[Cu(\mathbf{1})]^{2+}$. The cathodic (black) and anodic (red) absolute peak currents were found to scale linearly with scan rate, indicating the analyte to be surface-bound, as reported for $[Cu(TPA)(H_2O)]^{2+}$.[26] Interestingly, the potentials of $[Cu(\mathbf{1})]^{2+}$ redox peaks are dependent on ln(scan rate), although $E_{1/2}$ values remain constant. Figure 3d shows the linear dependence of both the cathodic (black) and anodic (red) absolute peak potentials on ln(scan rate). This linearity is interpreted using expressions 1 and 2 derived from the Butler−Volmer equation to calculate the symmetry factors (αn and $(1-\alpha)n$), charge transfer coefficient (α), and apparent electron transfer rate constant (k_{app}).[59,60] Here, F is the Faraday constant, $\upsilon_{c,a}$ are the cathodic and anodic scan rates, respectively, T is the temperature, and R is the gas constant.

$$E_{pc} = E_c^0 - \left(\frac{RT}{\alpha nF}\right)\ln\left[\frac{\alpha nF\upsilon_c}{RTk_{app}}\right] \quad (1)$$

$$E_{pa} = E_a^0 - \left(\frac{RT}{(1-\alpha)nF}\right)\ln\left[\frac{(1-\alpha)nF\upsilon_a}{RTk_{app}}\right] \quad (2)$$

The cathodic αn and the anodic $(1-\alpha)n$ were calculated from the slopes of the black and red dashed lines to be 0.43 and 0.72, respectively (Figure 3d). The sum of the two symmetry factors (1.15) is close to that expected for a reversible 1e$^-$ redox event (1.0).[61] Assuming a single electron transfer (n = 1), the average charge transfer coefficient (α = 0.35) indicates the energy barrier of the Cu(I/II) couple to be slightly asymmetric.[62] The y-intercepts correspond to the rate constants with cathodic k_{app} = 1.5 s^{-1} and anodic k_{app} = 2.0 s^{-1}. These rate constants are very low relative to 6 × 10^8 s^{-1} for an outer-sphere electron transfer (ET) process of ferrocene/ferrocenium ($Fc^{0/+}$) tethered to a Au surface with a short-chain thiolate,[63] and even small relative to 73.7 s^{-1} for a proton-coupled electron transfer (PCET) process for a quinone-derivative tethered to a Au electrode via a short-chain thiolate.[61] However, the rates seen in Cu complexes of **1**, **2**, **3**, **4**, and **5** (Figure 4) are comparable to those obtained for $Fc^{0/+}$ linked to Au via a *long-chain* thiolate (2.1 s^{-1}).[64] The slowness is likely associated with the complex undergoing an inner-sphere ET process with major

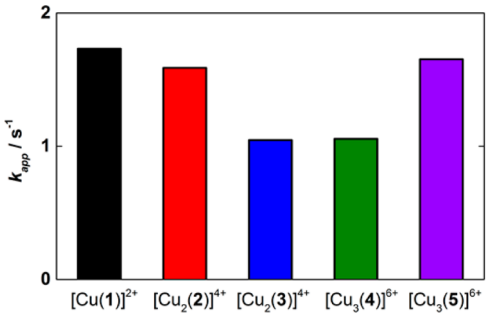

Figure 4. Apparent electron transfer rate constants (k_{app}) of $[Cu(\mathbf{1})]^{2+}$ (black), $[Cu_2(\mathbf{2})]^{4+}$ (red), $[Cu_2(\mathbf{3})]^{4+}$ (blue), $[Cu_3(\mathbf{4})]^{6+}$ (green), and $[Cu_3(\mathbf{5})]^{6+}$ (purple).

reorganization in coordination geometry, as suggested by the asymmetric energy barrier of the Cu(I/II) couple.[65,66] Also, ET rate may be further attenuated by the nature of a heterogeneous electrode surface with physisorbed Cu complexes bound inside a carbon−Nafion matrix.

3.1.2. Rotating Ring-Disk Electrode (RRDE) Measurements under O_2. Figure 5 depicts RRDE measurements obtained for Vulcan-supported $[Cu(\mathbf{1})]^{2+}$ at various pH values and in the presence of various anions. $[Cu(\mathbf{1})]^{2+}$ exhibits an ORR onset potential, defined as the potential at which 5% of the diffusion-limited current is reached, of 0.41 V vs RHE at pH 1 (Figure 5a). The observed ORR onset potential for $[Cu(\mathbf{1})]^{2+}$ is 120 mV more negative than $[Cu(TPA)(H_2O)]^{2+}$, which is presently the best synthetic Cu ORR catalyst at pH 1.[26] In the pH 4−7 range, $[Cu(\mathbf{1})]^{2+}$ exhibits ORR onset potentials ∼100 mV more negative than [Cu(2,9-dimethyl-1,10-phenanthroline)]$^{2+}$ on graphite, which is one of the Cu ORR catalysts with the lowest ORR overpotential in the pH 4−7 range.[67−70] In the pH 10−13 range, $[Cu(\mathbf{1})]^{2+}$ exhibits ORR onset potentials ∼140 mV more negative than the dinuclear Cu complex of 3,5-diamino-1,2,4-triazole, which is the benchmark synthetic Cu ORR catalyst between pH 10−13.[71] The ORR activity of $[Cu(\mathbf{1})]^{2+}$ is unaffected by changing the counteranion used in the preparation step, e.g., ClO_4^-, NO_3^-, SO_4^{2-}, Cl^-, HCO_2^-, and AcO^- (Figure 5b)—neither Lewis basicity nor charge has any effect on ORR activity.

As the pH is varied between 1 and 13 for $[Cu(\mathbf{1})]^{2+}$, the maximum amount of H_2O_2 detected ranges from 13% to 5.4% (Figure 6a, black), while the amount of H_2O_2 detected in the diffusion-limited region ranges from 3.0% to 1.0%. The complex $[Cu(TPA)(H_2O)]^{2+}$ exhibited comparable results.[26] Koutecky−Levich analysis of the RRDE data allows the determination of the number of electrons transferred during the ORR (SI Figure S1a−c). Over the pH 1−13 range, about 4 e$^-$ are transferred per catalytic cycle in the diffusion-limited current region, indicating that $[Cu(\mathbf{1})]^{2+}$ reduces O_2 to H_2O (Figure 6b, black). A correlation exists between the ORR onset potentials of the present system and the pH of the bulk solution (Figure 6c, black), with the potential scaling linearly by about 30 mV/pH. This correlation suggests that the rate-determining step involves protonation, as is characteristic of PCET processes.[72−77] Indeed, the onset potentials of all nonprecious metal catalysts examined to date exhibit pH dependence.[23,78,79] Notably, the shape of the voltammogram varies with pH (Figure 5a). In acidic medium, $[Cu(\mathbf{1})]^{2+}$ exhibits a Tafel slope of about 100 mV/dec (Figure 6d, black), which is close to the 120 mV/dec one would expect for a 1 e$^-$ rate-determining step as observed for $[Cu(\mathbf{1})]^{2+}$ at pH 1.[26] At pH 10−13, the Tafel

dx.doi.org/10.1021/ic501080c | Inorg. Chem. 2014, 53, 8505−8516

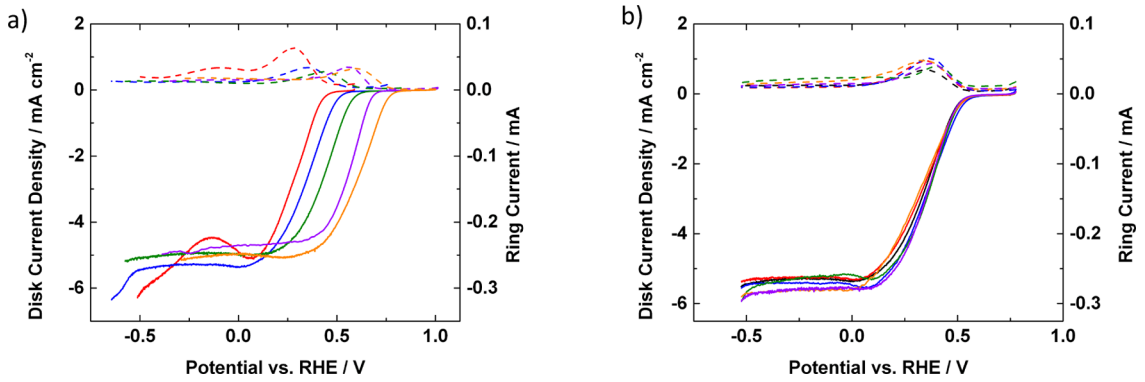

Figure 5. (a) Rotating ring-disk electrode (RRDE) experiments of $[Cu(\mathbf{1})]^{2+}$ in pH 1 (red), 4 (blue), 7 (green), 10 (purple), and 13 (orange) O_2-sparged solutions at 1600 rpm with a scan rate of 10 mV/s. (b) RRDE experiments of $[Cu(\mathbf{1})]^{2+}$ in pH 4 O_2-sparged Britton-Robinson buffer solution at 1600 rpm with a scan rate of 10 mV/s with ClO_4^- (black), NO_3^- (red), SO_4^{2-} (blue), Cl^- (green), HCO_2^- (orange), and AcO^- (purple) as counterions.

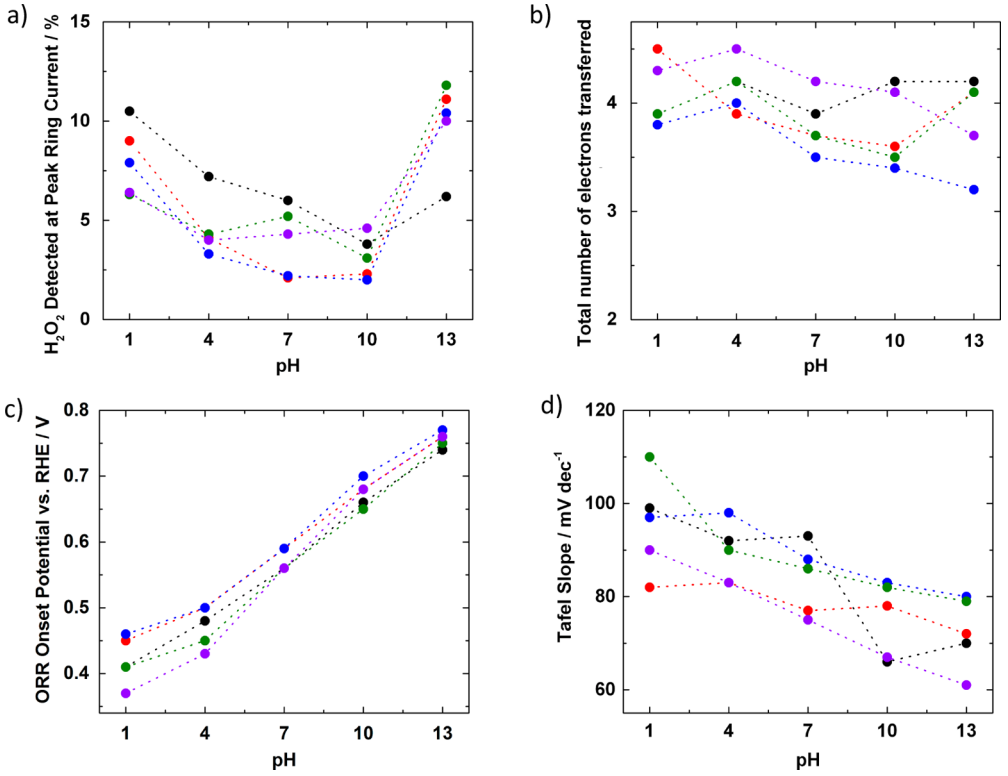

Figure 6. Plots of (a) peak percentages of H_2O_2 detected by the Pt ring, (b) total number of electrons transferred per catalytic cycle in the diffusion-limited region calculated from Koutecky–Levich analyses, (c) ORR onset potentials obtained from RRDE measurements, and (d) Tafel slopes acquired from linear sweep voltammograms (LSVs) of $[Cu(\mathbf{1})]^{2+}$ (black), $[Cu_2(\mathbf{2})]^{4+}$ (red), $[Cu_2(\mathbf{3})]^{4+}$ (blue), $[Cu_3(\mathbf{4})]^{6+}$ (green), and $[Cu_3(\mathbf{5})]^{6+}$ (purple) vs pH of the bulk solution.

slopes of $[Cu(\mathbf{1})]^{2+}$ decrease to about 70 mV/dec (Figure 6d, black), consistent with a $2e^-$ rate-determing step. This change was not observed for Cu systems of TPA and related derivatives.[27] A change in the Tafel slope is usually associated with a change in mechanism.[80]

3.1.3. Summary of Mononuclear Cu Complex. $[Cu(\mathbf{1})]^{2+}$ exhibits a well-defined redox couple under an Ar atmosphere and catalyzes the ORR at an overpotential slightly larger than that for $[Cu(TPA)(H_2O)]^{2+}$. Both the RRDE measurements and the Koutecky–Levich analysis suggest that $[Cu(\mathbf{1})]^{2+}$ effects $4e^-$ reduction of O_2, mirroring the activity of the analogous $[Cu(TPA)(H_2O)]^{2+}$. In acidic media, the Tafel behavior of $[Cu(\mathbf{1})]^{2+}$ is comparable to that of $[Cu(TPA)(H_2O)]^{2+}$, further supporting the use of DPA to replace TPA as a viable T3-site mimic for the rest of this study.

3.2. Dinuclear Systems: Cu Complexes with Linked DPA Units. *3.2.1. Voltammetry under Ar.* The Cu–Cu cooperativity implicit in the multicopper oxidases inspired us to test ligands incorporating two DPA moieties. Figure 7a shows the DPVs of the dicopper(II) complexes of **2** and **3**. Both complexes exhibit a single redox wave at about 0.25 V vs RHE, a value similar to that for the $[Cu(\mathbf{1})]^{2+}$ system (Figure 3c), thus indicating that the sites are equivalent.

3.2.2. RRDE Measurements under O_2. Figure 7b presents LSVs and RRDE measurements of $[Cu_2(\mathbf{2})]^{4+}$ and $[Cu_2(\mathbf{3})]^{4+}$. The ORR onset potentials and the diffusion-limited currents for

dx.doi.org/10.1021/ic501080c | Inorg. Chem. 2014, 53, 8505–8516

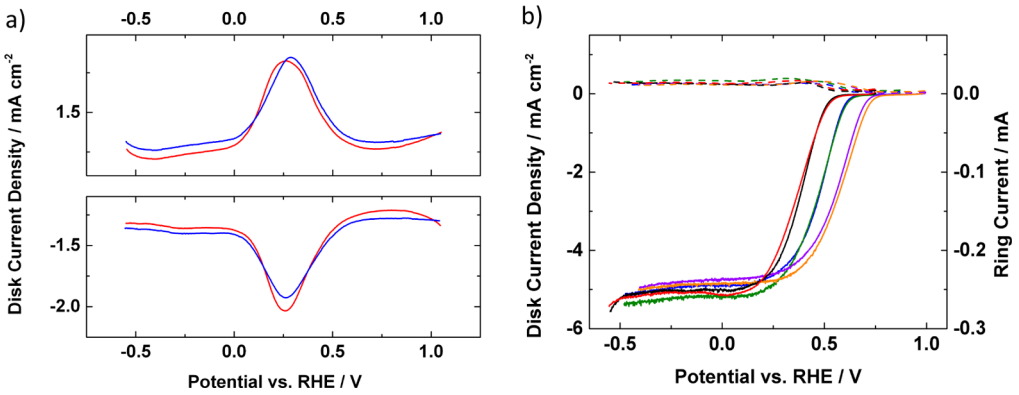

Figure 7. (a) DPVs for dinuclear complexes $[Cu_2(\mathbf{2})]^{4+}$ (red) and $[Cu_2(\mathbf{3})]^{4+}$ (blue) in pH 4 Ar-sparged Britton-Robinson buffer solution. (b) RRDE experiments for $[Cu_2(\mathbf{2})]^{4+}$ in pH 4 (black), pH 7 (blue), and pH 10 (purple), and $[Cu_2(\mathbf{3})]^{4+}$ in pH 4 (red), pH 7 (green), and pH 10 (orange) O_2-sparged Britton-Robinson buffer solution at 1600 rpm with a scan rate of 10 mV/s.

$[Cu_2(\mathbf{2})]^{4+}$ (Figure 7b, black) and $[Cu_2(\mathbf{3})]^{4+}$ (Figure 7b, red) are similar to those of $[Cu(\mathbf{1})]^{2+}$ at pH 4 (Figure 5a, blue). At pH 7 and 10, the ORR onset potentials for $[Cu_2(\mathbf{2})]^{4+}$ (Figure 7b, blue and purple) and $[Cu_2(\mathbf{3})]^{4+}$ (Figure 7b, green and orange) are about 20 mV more positive than those of $[Cu(\mathbf{1})]^{2+}$ (Figure 5a, green and purple). However, the slight differences observed in the diffusion-limited currents can be attributed to variation in different ink casts onto the GC electrode. The dicopper complexes produce less H_2O_2 (Figure 7b, dashed lines), indicating that they mediate $4e^-$ reduction even in the Tafel region.

Figure 6b summarizes the Koutecky–Levich results for $[Cu_2(\mathbf{2})]^{4+}$ (red) and $[Cu_2(\mathbf{3})]^{4+}$ (blue). The complexes catalyze $4e^-$ reduction of O_2 in the diffusion-limited region (SI Figure S2a–c and S3a–c), with a pH dependence (~30 mV/pH, Figure 6c) for the ORR onset in both $[Cu_2(\mathbf{2})]^{4+}$ (red) and $[Cu_2(\mathbf{3})]^{4+}$ (blue) systems. As expected, the Tafel slopes for $[Cu_2(\mathbf{2})]^{4+}$ (red) and $[Cu_2(\mathbf{3})]^{4+}$ (blue) vary with the bulk solution pH (Figure 6d). Taken together, these results show that the ORR activities of the dicopper complexes are similar if not identical to that of the mononuclear system.

3.2.3. Crystal Structures of Dinuclear Cu Complex of 3 before and after Oxygenation. To gain further insights into the reactivity displayed by $[Cu_2(\mathbf{2})]^{4+}$ and $[Cu_2(\mathbf{3})]^{4+}$, two examples of these species were examined crystallographically. The structure of $[Cu_2Cl_4(\mathbf{3})]$ reveals a centrosymmetric complex with two equivalent Cu centers linked by the polymethylene chain (Figure 8).

The coordination geometry of each Cu(II) is best described as a distorted square pyramidal, with the Addison τ parameter (the difference between the angles Cl1–Cu1–N1 and N2–Cu1–N3 divided by 60°) being 0.08, indicating a low degree of trigonality. Jahn–Teller distortion is indicated by the apical Cl2 being more distant from the metal center (2.511(4) Å) than is the basal Cl1 (2.254(1) Å). The intercopper distance is large at 10.500(8) Å, but the linker is flexible.

As expected for copper(II) species, $[Cu_2Cl_4(\mathbf{3})]$ is unreactive toward O_2. The relevant reactivity was thus sought with the analogous dicopper(I) complex, which was generated by combining $[Cu(MeCN)_4]BF_4$ and **3** (0.5 equiv). The product $[Cu_2(MeCN)_2(\mathbf{3})](BF_4)_2$ is a pale-yellow solid, exhibiting characteristic ^1H NMR and ESI-MS data. The material is extremely sensitive to air. Exposure of $[Cu_2(MeCN)_2(\mathbf{3})](BF_4)_2$ in MeCN solution to O_2 (1 atm) instantaneously afforded a green-blue solution, an identical observation also

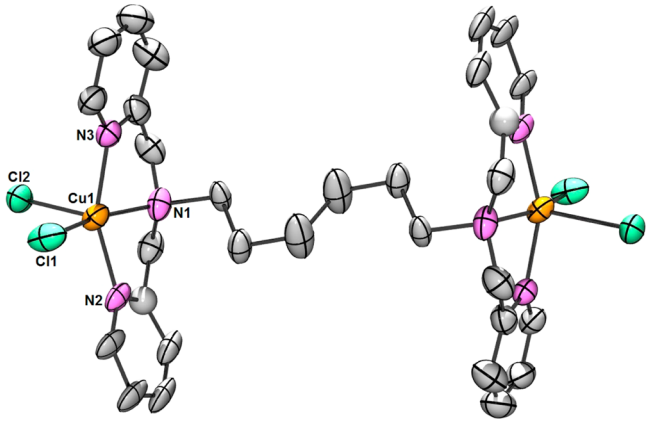

Figure 8. ORTEP of $[Cu_2Cl_4(\mathbf{3})]\cdot 2H_2O$ with ellipsoids drawn at the 50% probability level. The solvate molecules and H atoms are omitted for clarity. Selected distances (Å): Cu1–N1, 2.058(2); Cu1–N2, 2.026(6); Cu1–N3, 2.013(2); Cu1–Cl1, 2.254(1); Cu1–Cl2, 2.511(4). Selected angles (deg): Cl1–Cu1–N1, 160.87(7); N2–Cu1–N3, 155.9(5).

being found if the experiment was conducted at low temperature (−78 °C). Analysis of the solution by ESI-MS allowed for the detection of the cation $\{[Cu_2(OH)_2(\mathbf{3})]BF_4\}^+$ (m/z 727.0). This dinuclear species was thought to form upon the cleavage of O_2 by the cooperative active of two copper species, the metal centers of which are concomitantly oxidized to the Cu(II) state. The origin of the OH^- atoms is unclear, and $H^\bullet$ abstraction from MeCN or adventitious H_2O cannot be ruled out. Layering the MeCN solution with Et_2O garnered blue-green single crystals suitable for X-ray diffraction, the results of this analysis being presented in Figure 9.

While disordered solvent, counterions, and polymethylene chains resulted in the crystal data being relatively poor, the connectivity of the rather surprising $[Cu_4(OH)_4(\mathbf{3})_2](BF_4)_4$ product could be ascertained. The species can be viewed as a tetranuclear metallacycle incorporating two **3** ligands and four copper centers, each being ligated to a DPA fragment as well as two bridging OH^- groups in a distorted square pyramidal coordination geometry (τ_{Cu1} = 0.26, τ_{Cu2} = 0.26). The hydroxyl H atoms were located in the difference map, with further confirmation being found in O–H···F-BF_3^- interactions (O2–F4 @ 2.879(6) Å) and the average Cu–O distances (1.929(8) Å). Thus, the metallacycle features two Cu(II)(μ-OH)$_2$Cu(II) units that, along with related Cu(II)(μ-O_2)Cu(II) and

dx.doi.org/10.1021/ic501080c | Inorg. Chem. 2014, 53, 8505–8516

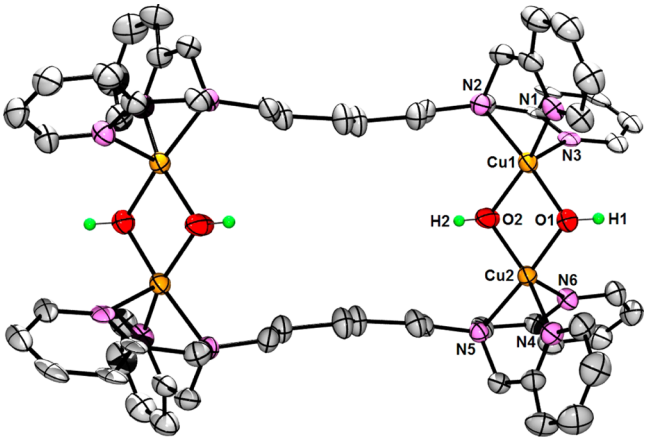

Figure 9. ORTEP of $[Cu_4(OH)_4(\mathbf{3})_2](BF_4)_4{\cdot}4MeCN{\cdot}4H_2O$ with ellipsoids drawn at the 50% probability level. The BF_4^- anions, solvate molecules and nonhydroxyl H atoms are omitted for clarity. Selected distances (Å): Cu1–O1, 1.926(2); Cu1–O2, 1.927(2); Cu1–N1, 2.010(3); Cu1–N2, 2.049(2); Cu1–N3, 2.272(5); Cu2–O1, 1.938(2); Cu2–O2, 1.924(2); Cu2–N4, 1.997(4); Cu2–N5, 2.071(2); Cu2–N6, 2.254(2); Cu1–Cu2, 2.9361(5), 10.0917(6). Selected angles (deg): Cu1–O1–Cu2, 98.92(9); Cu1–O2–Cu2, 99.35(9); O1–Cu1–N1, 96.2(2); O2–Cu1–N3, 105.8(4); O1–Cu2–N4, 95.8(3); O2–Cu2–N5, 97.36(8).

$Cu(III)(\mu\text{-}O)_2Cu(III)$ cores, are common motifs in copper enzymes.[17,81−83] The tetranuclear solid state structure contrasts the dinuclear species identified by ESI-MS, and it is possible that the dinuclear species "wraps" together to bind O_2 and further dimerizes to relieve ring strain. Alternatively, the dicopper(I) complex elongates (the polymethylene chain adopts a more staggered conformation relative to that in $[Cu_2Cl_4(\mathbf{3})]{\cdot}2H_2O$) and functions in concert with an additional dicopper species. It is interesting to note that exposure of the shorter analogue $[Cu_2(MeCN)_2(\mathbf{2})](BF_4)_2$ to O_2 afforded, in addition to an ion assigned to a dihydroxo dicopper(II) fragment (m/z 306.6), detection of the tetracopper complex (m/z 699.2, 437.9). Clearly, the shorter derivative favors the formation of a tetranuclear species, as a single dinculear species with a shorter linker is not suited to "wrapping" around to bind O_2.

3.2.4. Summary of Dinuclear Cu Complexes. The complexes $[Cu_2(\mathbf{2})]^{4+}$ and $[Cu_2(\mathbf{3})]^{4+}$ exhibit very similar ORR activity (*vide supra*). Crystal structures of the Cu complex of **3** before and after oxygenation provide clues to the reactivity of these complexes. The analyses indicate that the dicopper complex of **3** (and likely the dicopper complex of **2**) reacts with O_2 at the T3 DPA sites intermolecularly. This chemistry is reminiscent of the Kitagawa system, in which two {Cu[tri[2-(6-picolyl)]amine]}$^+$ units bind O_2 to afford the peroxodicopper(II) species $\{Cu_2[tri(6\text{-picolyl})methane)]_2(\mu\text{-}\eta^2\text{:}\eta^2\text{-}O_2)\}^{2+}$,[82,84,85] and other systems involving TPA derivatives observed by Karlin and Fukuzumi.[86] Kodera reported a more stable peroxodicopper(II) complex, in which tethered tridentate sites hold the Cu centers in close proximity, leading to enhanced (and *reversible*) O_2 binding.[87−89] Notably, the Kodera complexes have negligible ORR activity,[26] while the dinuclear

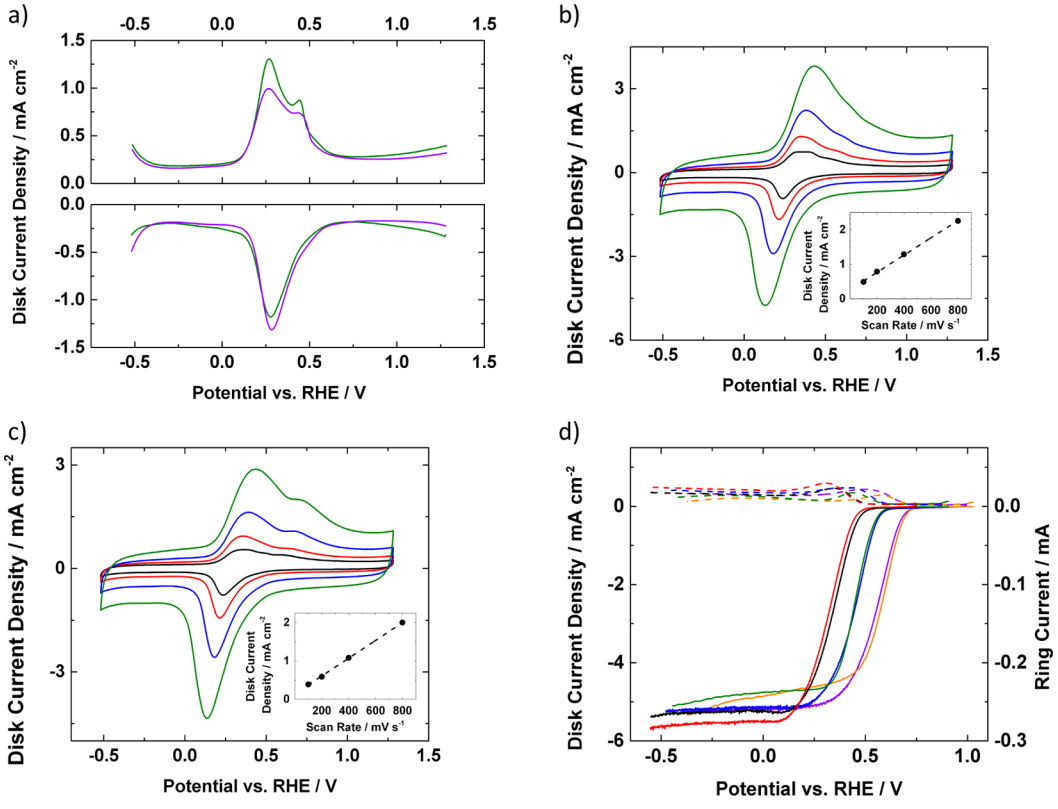

Figure 10. DPVs (a) of trinuclear complexes $[Cu_3(\mathbf{4})]^{6+}$ (green) and $[Cu_3(\mathbf{5})]^{6+}$ (purple). CVs of $[Cu_3(\mathbf{4})]^{6+}$ (b) and $[Cu_3(\mathbf{5})]^{6+}$ (c) with scan rates of 100 (black), 200 (red), 400 (blue), 800 (green) mV/s. Randles–Sevcik plots of $[Cu_3(\mathbf{4})]^{6+}$ (b, inset) and $[Cu_3(\mathbf{5})]^{6+}$ (c, inset) projected from the anodic (black circles) current densities of the peak/shoulder at above 0.5 V vs RHE. These three studies were conducted in pH 4 Ar-sparged Britton-Robinson buffer solutions. (d) RRDE data for $[Cu_3(\mathbf{4})]^{6+}$ in pH 4 (black), pH 7 (blue), and pH 10 (purple), and $[Cu_3(\mathbf{5})]^{6+}$ in pH 4 (red), pH 7 (green), and pH 10 (orange) O_2-sparged Britton-Robinson buffer solution at 1600 rpm with a scan rate of 10 mV/s.

dx.doi.org/10.1021/ic501080c | Inorg. Chem. 2014, 53, 8505−8516

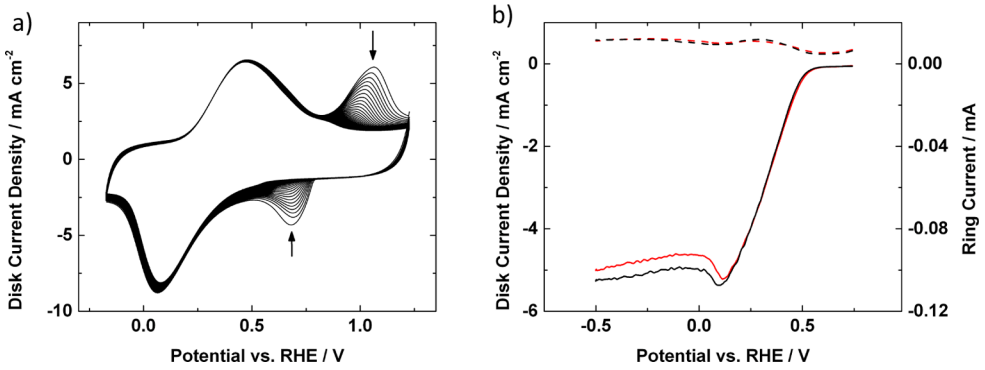

Figure 11. (a) CVs of $[AgCu_2(\mathbf{4})]^{5+}$ in pH 4 Ar-sparged Britton-Robinson buffer solution with a scan rate of 200 mV/s for 50 cycles. (b) RRDE experiments of $[AgCu_2(\mathbf{4})]^{5+}$ in pH 4 O_2-sparged Britton-Robinson buffer solution at 1600 rpm with a scan rate of 10 mV/s before (black) and after (red) 50 cycles under Ar.

complexes reported here are catalytically competent, possibly a result of the *irreversible* nature of O_2 binding in the present case. We ascribe this high reactivity of DPA-bound copper(I) fragments to the inability of DPA to occupy three sites at a tetrahedrally coordinated copper(I); instead DPA is well-suited to bind copper(II) in a planar fashion.

3.3. Trinuclear Systems: Cu Complexes Bearing the T3−T2−T3 Paradigm. *3.3.1. Voltammetry under Ar.* In view of the tricopper active site present in several oxidases, we examined two tricopper complexes with pairs of DPA groups. Figure 10a reports the DPVs for $[Cu_3(\mathbf{4})]^{6+}$ and $[Cu_3(\mathbf{5})]^{6+}$. The cathodic scans (lower box) for both complexes reveal a single reduction at 0.28 V vs RHE, this reduction wave being attributed to reduction of all cupric centers to the cuprous state. The anodic scan of $[Cu_3(\mathbf{4})]^{6+}$ reveals *two* oxidation waves (Figure 10a, upper box, green). The oxidation at 0.27 V is assigned to the Cu(I/II) couple at the DPA site, on the basis of its similarity to that of $[Cu(\mathbf{1})]^{2+}$. The remaining event at 0.44 V is thus attributed to bipy-bound Cu(I/II). Analogous behavior was observed for $[Cu_3(\mathbf{5})]^{6+}$ (Figure 10a, upper box, purple), with waves at 0.27 (Cu(I/II)−DPA) and 0.45 V (Cu(I/II)-terpy). In Figure 10a, the ratio of the total reductive to oxidative charge is 1:1, supporting the hypothesis that the waves are reversible. Also in Figure 10a, the ratio of the area under the peak at 0.27 V to the other oxidative peak is about 2:1, confirming the distribution of the Cu ions in the ligand—one Cu ion at each of the two DPA sites and one Cu ion at the bipy or terpy site. Apart from electrochemical characterization techniques, mass spectrometry of the tricopper complexes and elemental analysis of the tricopper complexes physisorbed on Vulcan XC-72 both confirm the Cu:ligand ratio to be 3:1.

Cyclic voltammograms and Randles−Sevcik plots for trinuclear complexes $[Cu_3(\mathbf{4})]^{6+}$ (Figure 10b) and $[Cu_3(\mathbf{5})]^{6+}$ (Figure 10c) were analyzed to establish their redox properties. The Randles−Sevcik plots (insets) show the linear relationship between the oxidative peaks/shoulders at about +0.7 V and the scan rate. This proportionality indicates that the oxidative peaks/shoulders are due to surface-bound redox centers. The similarity of the reductive and oxidative currents indicates reversibility.

3.3.2. RRDE Measurements under O_2. Figure 10d shows the LSVs and RRDE measurements for $[Cu_3(\mathbf{4})]^{6+}$ and $[Cu_3(\mathbf{5})]^{6+}$. At pH 4, the ORR onset potentials for $[Cu_3(\mathbf{4})]^{6+}$ (Figure 10d, black) and $[Cu_3(\mathbf{5})]^{6+}$ (Figure 10d, red) are about 30 mV more negative than that for $[Cu(\mathbf{1})]^{2+}$. At pH 7, both $[Cu_3(\mathbf{4})]^{6+}$ and $[Cu_3(\mathbf{5})]^{6+}$ exhibit onset potentials similar to that of $[Cu(\mathbf{1})]^{2+}$ and generate less H_2O_2 than $[Cu(\mathbf{1})]^{2+}$ (Figure 10d, blue and green lines). The diffusion-limited currents observed for $[Cu_3(\mathbf{4})]^{6+}$ and $[Cu_3(\mathbf{5})]^{6+}$ are similar to that for $[Cu(\mathbf{1})]^{2+}$ at both pH 4 and 7. At pH 10, $[Cu_3(\mathbf{4})]^{6+}$ (Figure 10d, purple) exhibits an ORR onset at ∼10 mV more negative than that for $[Cu(\mathbf{1})]^{2+}$, while $[Cu_3(\mathbf{5})]^{6+}$ (Figure 10d, orange) exhibits an ORR onset at ∼15 mV more positive and displays lower diffusion-limited currents than $[Cu(\mathbf{1})]^{2+}$, with all catalysts generating similar amounts of H_2O_2 (Figure 10d, purple and orange dashed lines) at pH 10.

To further understand the ORR activity of these trinuclear Cu complexes, we carried out Koutecky−Levich analyses on $[Cu_3(\mathbf{4})]^{6+}$ and $[Cu_3(\mathbf{5})]^{6+}$ (SI Figure S4a−c, S5a−c). As summarized in Figure 6b, the Koutecky−Levich analyses indicate transfer of $4e^-$ in the diffusion-limited regime throughout the pH 1−13 range, this being suggestive of H_2O production. Figure 6d reports the Tafel slopes of both complexes. Similar to $[Cu(\mathbf{1})]^{2+}$, $[Cu_2(\mathbf{2})]^{4+}$, and $[Cu_2(\mathbf{3})]^{4+}$, the Tafel slopes change from ∼100 mV/dec to ∼70 mV/dec These results indicate that $[Cu_3(\mathbf{4})]^{6+}$ and $[Cu_3(\mathbf{5})]^{6+}$ behave as ORR catalysts in the same way as $[Cu(\mathbf{1})]^{2+}$.

3.3.3. Metal Substitution Studies. We next investigated possible reasons that the ORR activity for these trinuclear Cu complexes is no better than that found with $[Cu(\mathbf{1})]^{2+}$. We were unable to obtain crystal structures of the trinuclear Cu complexes, in either oxygenated or deoxygenated form. From the similar ORR activities among the complexes of DPA and its derivatives, we hypothesize that the O_2 reduction process occurs at the DPA sites via an intermolecular pathway, with the third Cu (in either a bipy or terpy site) not participating in the ORR. To evaluate this claim, we conducted a series of electrochemical tests with trinuclear mixed metal complexes.

Given the greater affinity of DPA moieties for Cu(II) over Ag(I),[90] we generated $AgCu_2$ derivatives by treating 1:2 mixtures of the metal nitrates with **4**. It is predicted that two Cu(II) ions bind the tridentate DPA unit, with the Ag(I) ion coordinated to the bidentate bipy unit. Figure 11a shows the CV of $[AgCu_2(\mathbf{4})]^{5+}$ with two visible reversible waves. The Cu(I/II) couple of $[AgCu_2(\mathbf{4})]^{5+}$ at 0.25 V vs RHE is comparable to the redox couple of a Cu ion bound by a DPA unit, e.g. $[Cu(\mathbf{1})]^{2+}$, $[Cu_2(\mathbf{2})]^{4+}$, and $[Cu_2(\mathbf{3})]^{4+}$. The lack of an oxidative shoulder at 0.44 V vs RHE indicates that no Cu ion is present in the bipy unit. We assigned the remaining redox wave with an $E_{1/2}$ of 0.8 V vs RHE to be the Ag(0/I) couple of the $[AgCu_2(\mathbf{4})]^{5+}$. The ratio of the charges of the redox waves at 0.25 and 0.8 V vs RHE is 2:1, which matches the ratio

dx.doi.org/10.1021/ic501080c | Inorg. Chem. 2014, 53, 8505−8516

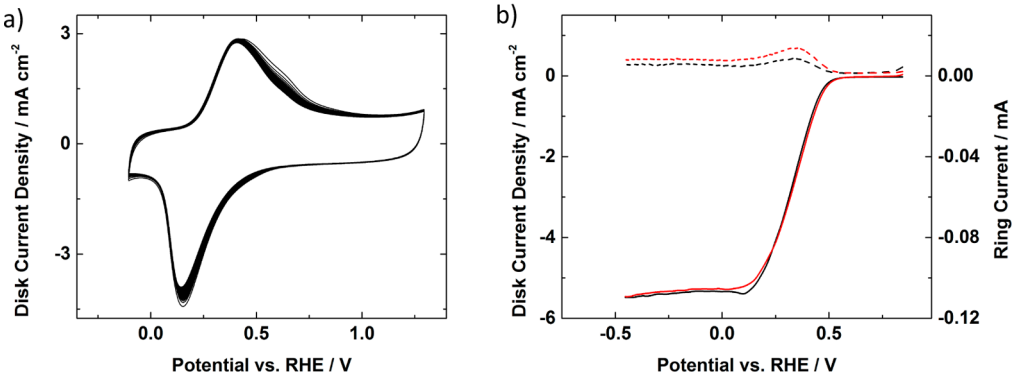

Figure 12. (a) CVs of $[Cu_2(\mathbf{4})]^{4+}$ in pH 4 Ar-sparged Britton-Robinson buffer solution with a scan rate of 200 mV/s for 50 cycles. (b) RRDE experiments of $[Cu_2(\mathbf{4})]^{4+}$ in pH 4 O_2-sparged Britton-Robinson buffer solution at 1600 rpm with a scan rate of 10 mV/s before (black) and after (red) 50 cycles under Ar.

determined from EA and ESI-MS data (m/z 1121.2 $[AgCu_2(NO_3)_4(\mathbf{4})]^+$). Taken together, the results confirm our proposed formulation of $[AgCu_2(\mathbf{4})]^{5+}$, with two Cu ions bound by the two DPA units of **4** and a Ag ion situated in the bipy pocket.

Figure 11b shows the LSVs of $[AgCu_2(\mathbf{4})]^{5+}$ with an ORR onset at 0.45 V vs RHE at pH 4, which is similar to those of $[Cu(\mathbf{1})]^{2+}$ and $[Cu_3(\mathbf{4})]^{6+}$. The amount of H_2O_2 detected by the ring (Figure 11b, black dashed line) and the diffusion-limited currents (Figure 11b, black solid line) of $[AgCu_2(\mathbf{4})]^{5+}$ are both comparable to those of $[Cu(\mathbf{1})]^{2+}$ and $[Cu_3(\mathbf{4})]^{6+}$. We then electrochemically removed the Ag(I) ions from the electrode surface by cycling for 50 times in the absence of O_2. Figure 11a shows the disappearance of the Ag(0/I) redox wave at 0.8 V vs RHE upon cycling. Figure 11b red lines show that the resulting complex exhibits ORR activity similar to that found before Ag leaching.

Control experiments were conducted with $[Cu_2(\mathbf{4})]^{4+}$. Mass spectrometry of $[Cu_2(\mathbf{4})]^{4+}$ and elemental analysis of $[Cu_2(\mathbf{4})]^{4+}$ physisorbed on Vulcan XC-72 both confirm the Cu:ligand ratio to be 2:1. Figure 12a shows the CV of $[Cu_2(\mathbf{4})]^{4+}$ under Ar. The redox wave at 0.25 V vs RHE is assigned to the Cu(I/II) couple for the Cu ions in the DPA sites, because the potential of the redox wave is similar to that of the Cu(I/II) couple observed for $[Cu(\mathbf{1})]^{2+}$ (*vide supra*). The lack of a redox wave at about 0.8 V vs RHE further confirms that such a wave observed in $[AgCu_2(\mathbf{4})]^{5+}$ is in fact due to the Ag(0/I) couple.

Figure 12b shows the LSVs of $[Cu_2(\mathbf{4})]^{4+}$ with an ORR onset at 0.45 V vs RHE at pH 4, which is similar to that of $[AgCu_2(\mathbf{4})]^{5+}$. The amount of H_2O_2 detected by the ring (Figure 12b, black dashed line) and the diffusion-limited current (Figure 12b, black solid line) are both comparable to that of $[AgCu_2(\mathbf{4})]^{5+}$. We then cycle $[Cu_2(\mathbf{4})]^{4+}$ for 50 times using the exact procedure for Ag leaching. The charge under the curve remains relatively constant (Figure 12a), suggesting that $[Cu_2(\mathbf{4})]^{4+}$ does not degrade over the course of the experiment. Figure 12b shows the linear voltammogram (red solid line) and RRDE measurements (red dashed line) of $[Cu_2(\mathbf{4})]^{4+}$ after potential cycling. The ORR activities of the postcycled and the precycled $[Cu_2(\mathbf{4})]^{4+}$ are comparable, suggesting there is minimal degradation resulting from potential cycling.

3.3.4. Summary of Trinuclear Cu Complexes. Cu complexes of **4**, in which the bipy site is vacant, or occupied by Cu or Ag, exhibit very similar ORR activity, suggesting that metal ions in the T2-mimicking site of our ligand do not actively engage in ORR. Hence, we hypothesize that trinuclear complexes $[Cu_3(\mathbf{4})]^{6+}$ and $[Cu_3(\mathbf{5})]^{6+}$ also react with O_2 through the T3 DPA sites via an intermolecular pathway, i.e. in a fashion similar to that of dinuclear complexes $[Cu_2(\mathbf{2})]^{4+}$ and $[Cu_2(\mathbf{3})]^{4+}$ and mononuclear complex $[Cu(\mathbf{1})]^{2+}$.

4. CONCLUSIONS

The ORR activity of $[Cu(\mathbf{1})]^{2+}$ is comparable to that of $[Cu(TPA)(H_2O)]^{2+}$ previously reported by our group. However, the ET rate between $[Cu(\mathbf{1})]^{2+}$ and the electrode surface is low, indicating that more intimate coupling to the electrode may be required for efficient ORR. Covalently linking two $[Cu(DPA)]^{2+}$ cores together results in ORR activities no better than $[Cu(\mathbf{1})]^{2+}$ alone. Crystallographic studies confirm the competency of dinuclear complexes $[Cu_2(\mathbf{2})]^{4+}$ and $[Cu_2(\mathbf{3})]^{4+}$ to activate O_2, although no advantage is conferred by linking the Cu sites. The challenges in this area are further illustrated by our tests on DPA as a synthon for the T3 sites, and bipy or terpy for the T2 site. However, trinuclear complexes $[Cu_3(\mathbf{4})]^{6+}$ and $[Cu_3(\mathbf{5})]^{6+}$ did not exhibit enhanced ORR activity, as compared to $[Cu(\mathbf{1})]^{2+}$. We show via metal substitution that the metal in the T2 equivalent site does not participate in the ORR process. Hence, more elaborate ligand design is imperative to fully mimic both the intricate structure of the active site of laccase and the remarkable ORR activity of laccase. The relationship of intersite flexibility and cooperativity is long recognized;[91] it is insufficient to simply connect reactive Cu sites. To ensure cooperativity comparable to that of metalloproteins, future catalysts require more sophisticated designs than those tested in this report.

■ ASSOCIATED CONTENT

Ⓢ Supporting Information

Additional information including Koutecky–Levich plots, Tafel plots, and NMR spectra as discussed in the text. This material is available free of charge via the Internet at http://pubs.acs.org.

■ AUTHOR INFORMATION

Corresponding Author

*Tel: 217-333-8329. Fax: 217-244-3186. E-mail: agewirth@illinois.edu.

Notes

The authors declare no competing financial interest.

dx.doi.org/10.1021/ic501080c | *Inorg. Chem.* 2014, 53, 8505−8516

■ ACKNOWLEDGMENTS

E.C.M.T. acknowledges a Croucher Foundation Scholarship. This research was supported under contract from the U.S. Department of Energy (DE-FG02-95ER46260).

■ REFERENCES

(1) Mehta, V.; Cooper, J. S. *J. Power Sources* **2003**, *114*, 32−53.
(2) Thomas, C. E. *Int. J. Hydrogen Energy* **2009**, *34*, 6005−6020.
(3) Sandy Thomas, C. E. *Int. J. Hydrogen Energy* **2009**, *34*, 9279−9296.
(4) Campanari, S.; Manzolini, G.; Garcia de la Iglesia, F. *J. Power Sources* **2009**, *186*, 464−477.
(5) Gewirth, A. A.; Thorum, M. S. *Inorg. Chem.* **2010**, *49*, 3557−3566.
(6) Gervasio, D. In *Encyclopedia of Electrochemical Power Sources*; Garche, J., Ed.; Elsevier: Amsterdam, 2009; pp 806−809.
(7) Wu, J.; Yuan, X. Z.; Martin, J. J.; Wang, H.; Zhang, J.; Shen, J.; Wu, S.; Merida, W. *J. Power Sources* **2008**, *184*, 104−119.
(8) Li, H.; Shi, Z.; Zhang, J. In *Encyclopedia of Electrochemical Power Sources*; Garche, J., Ed.; Elsevier: Amsterdam, 2009; pp 941−950.
(9) Li, H.; Tang, Y.; Wang, Z.; Shi, Z.; Wu, S.; Song, D.; Zhang, J.; Fatih, K.; Zhang, J.; Wang, H.; Liu, Z.; Abouatallah, R.; Mazza, A. *J. Power Sources* **2008**, *178*, 103−117.
(10) Wu, J.; Yuan, X. Z.; Martin, J. J.; Wang, H. In *Encyclopedia of Electrochemical Power Sources*; Garche, J., Ed.; Elsevier: Amsterdam, 2009; pp 848−867.
(11) Bergens, S. H.; Markiewicz, M. E. P. In *Encyclopedia of Electrochemical Power Sources*; Garche, J., Ed.; Elsevier: Amsterdam, 2009; pp 616−625.
(12) Borup, R. L.; Davey, J. R.; Garzon, F. H.; Wood, D. L.; Inbody, M. A. *J. Power Sources* **2006**, *163*, 76−81.
(13) Cai, M.; Ruthkosky, M. S.; Merzougui, B.; Swathirajan, S.; Balogh, M. P.; Oh, S. H. *J. Power Sources* **2006**, *160*, 977−986.
(14) Shao, Y.; Yin, G.; Gao, Y. *J. Power Sources* **2007**, *171*, 558−566.
(15) Zhang, S.; Yuan, X.-Z.; Hin, J. N. C.; Wang, H.; Friedrich, K. A.; Schulze, M. *J. Power Sources* **2009**, *194*, 588−600.
(16) Blackman, A. G.; Tolman, W. B. *Struct. Bonding (Berlin)* **2000**, *97*, 179−211.
(17) Hatcher, L.; Karlin, K. *J. Biol. Inorg. Chem.* **2004**, *9*, 669−683.
(18) Mirica, L. M.; Ottenwaelder, X.; Stack, T. D. P. *Chem. Rev.* **2004**, *104*, 1013−1046.
(19) Lewis, E. A.; Tolman, W. B. *Chem. Rev.* **2004**, *104*, 1047−1076.
(20) Hatcher, L. Q.; Karlin, K. D. In *Advances in Inorganic Chemistry*; van Eldik, R., Reedijk, J., Eds.; Academic Press: 2006; Vol. *58*, pp 131−184.
(21) Cramer, C. J.; Tolman, W. B. *Acc. Chem. Res.* **2007**, *40*, 601−608.
(22) Dagys, M.; Haberska, K.; Shleev, S.; Arnebrant, T.; Kulys, J.; Ruzgas, T. *Electrochem. Commun.* **2010**, *12*, 933−935.
(23) Thorseth, M. A.; Tornow, C. E.; Tse, E. C. M.; Gewirth, A. A. *Coord. Chem. Rev.* **2013**, *257*, 130−139.
(24) Jensen, M. P.; Que, E. L.; Shan, X.; Rybak-Akimova, E.; Que, J. L. *Dalton Trans.* **2006**, 3523−3527.
(25) Karlin, K. D.; Wei, N.; Jung, B.; Kaderli, S.; Niklaus, P.; Zuberbuehler, A. D. *J. Am. Chem. Soc.* **1993**, *115*, 9506−9514.
(26) Thorseth, M. A.; Letko, C. S.; Rauchfuss, T. B.; Gewirth, A. A. *Inorg. Chem.* **2011**, *50*, 6158−6162.
(27) Thorseth, M. A.; Letko, C. S.; Tse, E. C. M.; Rauchfuss, T. B.; Gewirth, A. A. *Inorg. Chem.* **2013**, *52*, 628−634.
(28) Messerschmidt, A.; Luecke, H.; Huber, R. *J. Mol. Biol.* **1993**, *230*, 997−1014.
(29) Solomon, E. I.; Sundaram, U. M.; Machonkin, T. E. *Chem. Rev.* **1996**, *96*, 2563−2606.
(30) McGuirl, M. A.; Dooley, D. M. *Curr. Opin. Chem. Biol.* **1999**, *3*, 138−144.
(31) Hakulinen, N.; Andberg, M.; Kallio, J.; Koivula, A.; Kruus, K.; Rouvinen, J. *J. Struct. Biol.* **2008**, *162*, 29−39.
(32) Garavaglia, S.; Teresa Cambria, M.; Miglio, M.; Ragusa, S.; Iacobazzi, V.; Palmieri, F.; D'Ambrosio, C.; Scaloni, A.; Rizzi, M. *J. Mol. Biol.* **2004**, *342*, 1519−1531.
(33) Piontek, K.; Antorini, M.; Choinowski, T. *J. Biol. Chem.* **2002**, *277*, 37663−37669.
(34) Schweiger, H.; Vayner, E.; Anderson, A. B. *Electrochem. Solid-State Lett.* **2005**, *8*, A585−A587.
(35) Mano, N.; Soukharev, V.; Heller, A. *J. Phys. Chem. B* **2006**, *110*, 11180−11187.
(36) Pita, M.; Shleev, S.; Ruzgas, T.; Fernández, V. M.; Yaropolov, A. I.; Gorton, L. *Electrochem. Commun.* **2006**, *8*, 747−753.
(37) Blanford, C. F.; Heath, R. S.; Armstrong, F. A. *Chem. Commun.* **2007**, 1710−1712.
(38) Blanford, C. F.; Foster, C. E.; Heath, R. S.; Armstrong, F. A. *Faraday Discuss.* **2009**, *140*, 319−335.
(39) Thorum, M. S.; Anderson, C. A.; Hatch, J. J.; Campbell, A. S.; Marshall, N. M.; Zimmerman, S. C.; Lu, Y.; Gewirth, A. A. *J. Phys. Chem. Lett.* **2010**, *1*, 2251−2254.
(40) Murphy, M. E. P.; Lindley, P. F.; Adman, E. T. *Protein Sci.* **1997**, *6*, 761−770.
(41) Ducros, V.; Brzozowski, A. M.; Wilson, K. S.; Ostergaard, P.; Schneider, P.; Svendson, A.; Davies, G. J. *Acta Crystallogr., Sect D* **2001**, *57*, 333−336.
(42) Cracknell, J. A.; Vincent, K. A.; Armstrong, F. A. *Chem. Rev.* **2008**, *108*, 2439−2461.
(43) Toledo-Núñez, C.; López-Cruz, J. I.; Hernández-Arana, A. *Biophys. Chem.* **2012**, *167*, 36−42.
(44) St-Pierre, J. In *Encyclopedia of Electrochemical Power Sources*; Garche, J., Ed.; Elsevier: Amsterdam, 2009; pp 901−911.
(45) Hakulinen, N.; Kiiskinen, L.-L.; Kruus, K.; Saloheimo, M.; Paananen, A.; Koivula, A.; Rouvinen, J. *Nat. Struct. Mol. Biol.* **2002**, *9*, 601−605.
(46) Solomon, E. I.; Augustine, A. J.; Yoon, J. *Dalton Trans.* **2008**, 3921−3932.
(47) Casarin, M.; Corvaja, C.; Di Nicola, C.; Falcomer, D.; Franco, L.; Monari, M.; Pandolfo, L.; Pettinari, C.; Piccinelli, F. *Inorg. Chem.* **2005**, *44*, 6265−6276.
(48) Ouellette, W.; Yu, M. H.; O'Connor, C. J.; Hagrman, D.; Zubieta, J. *Angew. Chem., Int. Ed.* **2006**, *45*, 3497−3500.
(49) Maiti, D.; Woertink, J. S.; Ghiladi, R. A.; Solomon, E. I.; Karlin, K. D. *Inorg. Chem.* **2009**, *48*, 8342−8356.
(50) Palmer, A. E.; Lee, S. K.; Solomon, E. I. *J. Am. Chem. Soc.* **2001**, *123*, 6591−6599.
(51) Erturk, H.; Hofmann, A.; Puchta, R.; van Eldik, R. *Dalton Trans.* **2007**, 2295−2301.
(52) Suntharalingam, K.; Hunt, D. J.; Duarte, A. A.; White, A. J. P.; Mann, D. J.; Vilar, R. *Chem.—Eur. J.* **2012**, *18*, 15133−15141.
(53) Humphreys, K. J.; Karlin, K. D.; Rokita, S. E. *J. Am. Chem. Soc.* **2002**, *124*, 8055−8066.
(54) Choi, K.-Y.; Ryu, H.; Sung, N.-D.; Suh, M. *J. Chem. Crystallogr.* **2003**, *33*, 947−950.
(55) Bruker *APEX2*; Bruker AXS, Inc.: Madison, Wisconsin, U.S.A., 2010.
(56) Bruker *SAINT, SHELXTL, SADABS, XCIF, XPREP*; Bruker AXS, Inc.: Madison, Wisconsin, U.S.A., 2005.
(57) Sheldrick, G. M. *Acta Crystallogr.* **2008**, *A64*, 112−122.
(58) Spek, A. L.; van der Sluis, P. *Acta Crystallogr.* **1990**, *A46*, 194−201.
(59) Laviron, E. *J. Electroanal. Chem. Interfacial Electrochem.* **1979**, *101*, 19−28.
(60) Eckermann, A. L.; Feld, D. J.; Shaw, J. A.; Meade, T. J. *Coord. Chem. Rev.* **2010**, *254*, 1769−1802.
(61) Park, W.-C.; Hong, H.-G. *Bull. Korean Chem. Soc.* **2006**, *27*, 381−385.
(62) Bard, A. J.; Faulkner, L. R. *Electrochemical Methods: Fundamentals and Applications*; Wiley: New York, 2000.
(63) Smalley, J. F.; Feldberg, S. W.; Chidsey, C. E. D.; Linford, M. R.; Newton, M. D.; Liu, Y.-P. *J. Phys. Chem.* **1995**, *99*, 13141−13149.

(64) Hosseini, A.; Collman, J. P.; Devadoss, A.; Williams, G. Y.; Barile, C. J.; Eberspacher, T. A. *Langmuir* **2010**, *26*, 17674−17678.
(65) Rorabacher, D. B. *Chem. Rev.* **2004**, *104*, 651−698.
(66) Vande Linde, A. M. Q.; Westerby, B. C.; Ochrymowycz, L. A.; Rorabacher, D. B. *Inorg. Chem.* **1993**, *32*, 251−257.
(67) Zhang, J.; Anson, F. C. *Electrochim. Acta* **1993**, *38*, 2423−2429.
(68) Lei, Y.; Anson, F. C. *Inorg. Chem.* **1994**, *33*, 5003−5009.
(69) Lei, Y.; Anson, F. C. *Inorg. Chem.* **1995**, *34*, 1083−1089.
(70) McCrory, C. C. L.; Ottenwaelder, X.; Stack, T. D. P.; Chidsey, C. E. D. *J. Phys. Chem. A* **2007**, *111*, 12641−12650.
(71) Thorum, M. S.; Yadav, J.; Gewirth, A. A. *Angew. Chem., Int. Ed.* **2009**, *48*, 165−167.
(72) Cukier, R. I.; Nocera, D. G. *Annu. Rev. Phys. Chem.* **1998**, *49*, 337−369.
(73) Mayer, J. M. *Annu. Rev. Phys. Chem.* **2004**, *55*, 363−390.
(74) Madhiri, N.; Finklea, H. O. *Langmuir* **2006**, *22*, 10643−10651.
(75) Huynh, M. H. V.; Meyer, T. J. *Chem. Rev.* **2007**, *107*, 5004−5064.
(76) Rosenthal, J.; Nocera, D. G. *Acc. Chem. Res.* **2007**, *40*, 543−553.
(77) Weinberg, D. R.; Gagliardi, C. J.; Hull, J. F.; Murphy, C. F.; Kent, C. A.; Westlake, B. C.; Paul, A.; Ess, D. H.; McCafferty, D. G.; Meyer, T. J. *Chem. Rev.* **2012**, *112*, 4016−4093.
(78) Zhang, J.; Anson, F. C. *J. Electroanal. Chem.* **1992**, *341*, 323−341.
(79) Nagao, H.; Komeda, N.; Mukaida, M.; Suzuki, M.; Tanaka, K. *Inorg. Chem.* **1996**, *35*, 6809−6815.
(80) Fletcher, S. *J. Solid State Electrochem.* **2009**, *13*, 537−549.
(81) Mahapatra, S.; Kaderli, S.; Llobet, A.; Neuhold, Y. M.; Palanche, T.; Halfen, J. A.; Young, V. G.; Kaden, T. A.; Que, L.; Zuberbuhler, A. D.; Tolman, W. B. *Inorg. Chem.* **1997**, *36*, 6343−6356.
(82) Hayashi, H.; Fujinami, S.; Nagatomo, S.; Ogo, S.; Suzuki, M.; Uehara, A.; Watanabe, Y.; Kitagawa, T. *J. Am. Chem. Soc.* **2000**, *122*, 2124−2125.
(83) Cahoy, J.; Holland, P. L.; Tolman, W. B. *Inorg. Chem.* **1999**, *38*, 2161−2168.
(84) Mizuno, M.; Hayashi, H.; Fujinami, S.; Furutachi, H.; Nagatomo, S.; Otake, S.; Uozumi, K.; Suzuki, M.; Kitagawa, T. *Inorg. Chem.* **2003**, *42*, 8534−8544.
(85) Taki, M.; Teramae, S.; Nagatomo, S.; Tachi, Y.; Kitagawa, T.; Itoh, S.; Fukuzumi, S. *J. Am. Chem. Soc.* **2002**, *124*, 6367−6377.
(86) Fukuzumi, S.; Karlin, K. D. *Coord. Chem. Rev.* **2013**, *257*, 187−195.
(87) Kodera, M.; Kajita, Y.; Tachi, Y.; Katayama, K.; Kano, K.; Hirota, S.; Fujinami, S.; Suzuki, M. *Angew. Chem., Int. Ed.* **2004**, *43*, 334−337.
(88) Kodera, M.; Kano, K. *Bull. Chem. Soc. Jpn.* **2007**, *80*, 662−676.
(89) Kodera, M.; Katayama, K.; Tachi, Y.; Kano, K.; Hirota, S.; Fujinami, S.; Suzuki, M. *J. Am. Chem. Soc.* **1999**, *121*, 11006−11007.
(90) Zuckerman, J. J.; Hagen, A. P. *Inorganic Reactions and Methods, The Formation of Bonds to N,P,As,Sb,Bi*; Wiley: New York, 2009.
(91) Collman, J. P. *Acc. Chem. Res.* **1977**, *10*, 265−272.